Cite This: *Inorg. Chem.* XXXX, XXX, XXX–XXX

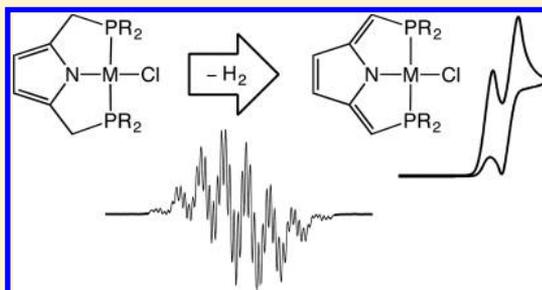# Backbone Dehydrogenation in Pyrrole-Based Pincer Ligands

V. Mahesh Krishnan,[‡] Ian Davis,[‡] Tessa M. Baker,[§] Daniel J. Curran,[§] Hadi D. Arman,[‡] Michael L. Neidig,[§] Aimin Liu,[‡] and Zachary J. Tonzetich*,[‡]

[‡]Department of Chemistry, University of Texas at San Antonio (UTSA), San Antonio, Texas 78249, United States
[§]Department of Chemistry, University of Rochester, Rochester, New York 14627, United States

S *Supporting Information*

ABSTRACT: Treatment of both $[CoCl(^{tBu}PNP)]$ and $[NiCl(^{tBu}PNP)]$ (^{tBu}PNP = anion of 2,5-bis((di-*tert*-butylphosphino)methyl)pyrrole) with one equivalent of benzoquinone affords the corresponding chloride complexes containing a dehydrogenated PNP ligand, $^{tBu}dPNP$ ($^{tBu}dPNP$ = anion of 2,5-bis((di-*tert*-butylphosphino)methylene)-2,5-dihydropyrrole). Dehydrogenation of PNP to dPNP results in minimal change to steric profile of the ligand but has important consequences for the resulting redox potentials of the metal complexes, resulting in the ability to isolate both $[CoH(^{tBu}dPNP)]$ and $[CoEt(^{tBu}dPNP)]$, which are more challenging (hydride) or not possible (ethyl) to prepare with the parent PNP ligand. Electrochemical measurements with both the Co and Ni dPNP species demonstrate a substantial shift in redox potentials for both the M(II/III) and M(II/I) couples. In the case of the former, oxidation to trivalent Co was found to be reversible, and subsequent reaction with $AgSbF_6$ afforded a rare example of a square-planar Co(III) species. Corresponding reduction of $[CoCl(^{tBu}dPNP)]$ with KC_8 produced the diamagnetic Co(I) species, $[Co(N_2)(^{tBu}dPNP)]$. Further reduction of the Co(I) complex was found to generate a pincer-based π-radical anion that demonstrated well-resolved EPR features to the four hydrogen atoms and lone nitrogen atom of the ligand with minor contributions from cobalt and coordinated N_2. Changes in the electronic character of the PNP ligand upon dehydrogenation are proposed to result from loss of aromaticity in the pyrrole ligand, resulting in a more reducing central amido donor. DFT calculations on the Co(II) complexes were performed to shed further insight into the electronic structure of the pincer complexes.

INTRODUCTION

The modularity of pincers is one of the most desirable attributes of this class of ligands and has been used to great effect in designing and optimizing molecular catalysts.[1−4] In addition to substitution of the groups on the donor atoms, modification of the pincer backbone has also emerged as an effective strategy for altering the electronic properties of the ligand as well as engaging the pincer itself in reaction chemistry. Two prominent examples of such pincer-based reactivity are deprotonation and redox noninnocence, both of which have been exploited in the design of catalysts featuring earth-abundant transition metals.[5−11]

Proton and electron transfer events involving pincer ligands are primarily relegated to neutral variants at present.[12−16] Notable examples featuring anionic pincers include the amide-based NNN/ONO ligands studied by Heyduk,[17−21] the asymmetric diamine-amido PN³P ligands developed by Huang,[22,23] the pyrrolide-oxazoline NNN ligands introduced by Gade,[2,24] the diiminopyrrole-derived NNN ligands recently prepared by Anderson,[25,26] and the aliphatic amine-based PNP ligands employed by Schneider.[27] In the latter case, removal of H_2 equivalents from the pincer backbone afforded modified ligands with higher degrees of unsaturation.[28,29] Unsurprisingly, these dehydrogenated ligands were found to be more electron-poor than their parent ligand, consistent with a formal oxidation process. In addition to these examples, the ubiquitous diarylamido-based PNP pincer is capable of ligand-based oxidation in certain instances,[30] and the pyrrole-based pincer ligands, pyr-ONO (pyr-ONO = trianion of 2,5-bis(3-(*tert*-butyl)2-phenoxy)pyrrole) and ^{tBu}PNP (^{tBu}PNP = anion of 2,5-bis((di-*tert*-butylphosphino)methyl)pyrrole), have been demonstrated to undergo protonation at the 3- and 4-positions of the pyrrolic ring in the presence of strong acids.[31,32]

In the context of our continuing interest in the pyrrole-based ^RPNP system,[33−38] we now describe a new modification to the ligand arising from dehydrogenation of the C_6 backbone (Scheme 1). A variety of transition metal complexes of ^RPNP

**Scheme 1. Dehydrogenation of the ^RPNP Ligand**
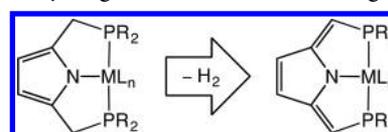
has already been reported to demonstrate unique reactivity and catalysis,[39−49] and alteration of the ligand framework promises to further expand the applications of this pincer system. In the present study, backbone dehydrogenation of ^{tBu}PNP is found to result in dramatic changes to the redox potentials of the corresponding Co and Ni complexes, permitting isolation of heretofore unisolable compounds in the case of cobalt(II). The ability to isolate these species is attributed to the more electron-rich nature of the dehydrogenated PNP ligand (dPNP). This counterintuitive result, whereby oxidation leads to a more electron-rich ligand, is ascribed to the loss of aromaticity in the pyrrole ring, leading to a more basic central amido donor.

■ RESULTS AND DISCUSSION

Ligand Dehydrogenation. In similar fashion to the dehydrogenation protocol reported by Schneider,[29] treatment of either [CoCl(^{tBu}PNP)] (**1-Cl**) or [NiCl(^{tBu}PNP)] (**2-Cl**) with one equivalent of 1,4-benzoquinone in benzene afforded the corresponding chloride complexes containing the dehy-

drogenated ligand, ^{tBu}dPNP (**1^d-Cl** and **2^d-Cl**, eq 1). ^{1}H and ^{13}C NMR analyses of the Ni analogue, **2^d-Cl**, demonstrated a shift in the resonances corresponding to the pyrrolic backbone and the methylene arms versus **2-Cl** (see Supporting Information). In addition, the integrated area for the hydrogen atoms of the pincer arms changed from four to two. Somewhat surprisingly, the ^{31}P NMR resonance of **2^d-Cl** was observed at 67.15 ppm, which is only a small shift from the value of 64.93 ppm found for **2-Cl**.[40] In similar fashion to the synthesis of **1^d-Cl** and **2^d-Cl**, attempted preparation of the iron(II) analogue, [FeCl(^{tBu}dPNP)], was unsuccessful, presumably due to oxidation of the iron center.
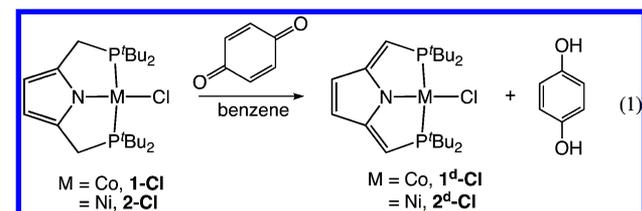
The solubility properties of both **1^d-Cl** and **2^d-Cl** are similar to those of **1-Cl** and **2-Cl**, permitting facile crystallization from concentrated pentane solutions at −30 °C. The solid-state structures of both compounds are shown in Figure 1. Notable metric parameters highlighting the differences between the ^{tBu}PNP and ^{tBu}dPNP ligands are compiled in Table 1.

Dehydrogenation of the PNP ligand minimally alters the metal−ligand bond distances and angles across all complexes, although both **1^d-Cl** and **2^d-Cl** are more rigidly planar than **1-Cl** and **2-Cl**. The most notable change in metal−ligand bond metrics occurs for the M(1)−N(1) distances, which are slightly shorter in **1^d-Cl** and **2^d-Cl** then they are in **1-Cl** and **2-Cl**. Despite these modest changes involving the metal center, significant structural changes in the ligand backbone accompany dehydrogenation. The C(5)−C(1), C(14)−C(4) (not shown), and C(2)−C(3) distances contract, whereas the C(1)−C(2) distance elongates, consistent with the structural representation of the ligand displayed in Scheme 1. The C−P bonds undergo a modest contraction upon dehydrogenation (Δ ∼ 0.05 Å) in line with the change in hybridization of C(5) and C(14) from sp^3 to sp^2. By contrast, the C−N distances are unchanged, reflecting the fact that carbon atoms C(1) and C(4) remain sp^2. In total, the C−C and C−N distances of **1^d-Cl** and **2^d-Cl** are consistent with those observed for a related dehydrogenated pyrazole-substituted dimethylpyrrole,[50] further supporting the depiction shown in Scheme 1.

Having structurally characterized compounds **1^d-Cl** and **2^d-Cl**, we next examined their electrochemical behavior. We envisioned that dehydrogenation of the PNP ligand would not only alter the electronics of the compounds markedly, but also potentially introduce new ligand-based redox events as a consequence of the higher degree of conjugation present in the dPNP backbone. The cyclic voltammograms of compounds **1^d-Cl** and **2^d-Cl** are displayed in Figure 2. Data for **1-Cl** is also plotted alongside that of **1^d-Cl** for comparison. As can be seen from the voltammograms of **1-Cl** and **1^d-Cl**, both compounds display a similar number of electrochemical events but with notable differences. Most apparent is the new reversible one-electron oxidation event at an $E_{1/2}$ of 0.03 V (vs Fc/Fc$^+$), which is shifted to lower potential from the corresponding irreversible process in **1-Cl**. In similar fashion, **2^d-Cl** displays a reversible one-electron oxidation at 0.15 V that is absent in **2-Cl**. In addition to the anodic events, the irreversible one-electron reduction events observed for **1-Cl** and **2-Cl** are also shifted to lower potential in compounds **1^d-Cl** and **2^d-Cl**. We ascribe these negative shifts in potential for both the M(II)/M(III) and M(II)/M(I) couples to the more basic nitrogen atom of dPNP that results from dearomatization of the pyrrole ring during dehydrogenation. Loss of aromaticity in the ring effectively liberates the nitrogen lone pairs, imparting more amido character to the central donor atom.

In addition to the metal-based redox events, **1^d-Cl** displays a reversible cathode process at −2.78 V that we propose originates from a ligand-based reduction in the compound
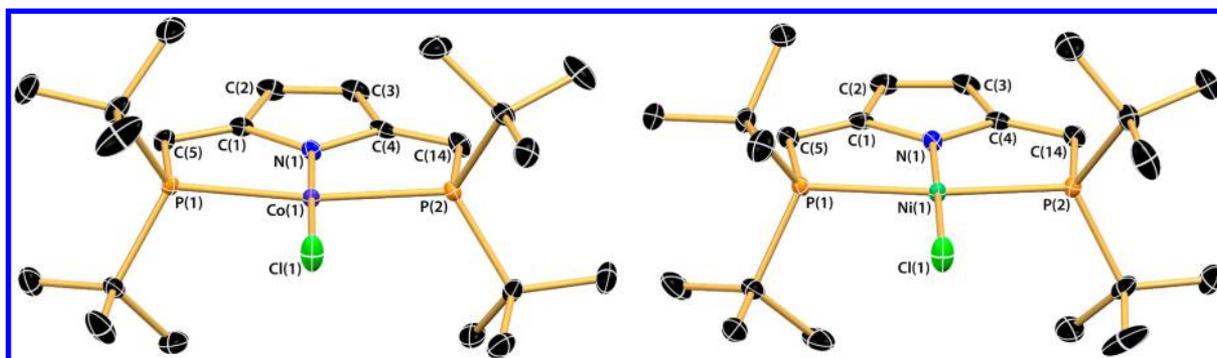
Figure 1. Thermal ellipsoid (50%) drawings of **1^d-Cl** (left) and **2^d-Cl** (right). Hydrogen atoms omitted for clarity.

Table 1. Comparison of Metric Parameters for Co and Ni Chloride Complexes[a]

bond	1-Cl	1^d-Cl	2-Cl	2^d-Cl
M(1)−N(1)	1.8626(16)	1.8434(15)	1.860(5)	1.8411(15)
M(1)−P$_{avg}$	2.246(1)	2.269(1)	2.227(2)	2.253(1)
M(1)−Cl(1)	2.2004(6)	2.2057(5)	2.1830(18)	2.1848(5)
P(1)−C(5)	1.851(2)	1.7990(19)	1.855(6)	1.7949(19)
C(5)−C(1)	1.500(3)	1.350(3)	1.489(8)	1.351(3)
C(1)−C(2)	1.364(3)	1.468(3)	1.389(7)	1.464(3)
C(2)−C(3)	1.419(3)	1.340(3)	1.428(10)	1.343(3)
C(1)−N(1)	1.385(2)	1.384(2)	1.384(7)	1.387(2)
P(1)−M(1)−P(2)	167.53(2)	165.47(2)	168.08(6)	165.97(2)

[a]Atom labels for all complexes are consistent with those in Figure 1. Metric parameters for **1-Cl** and **2-Cl** were obtained from references 44 and 40.
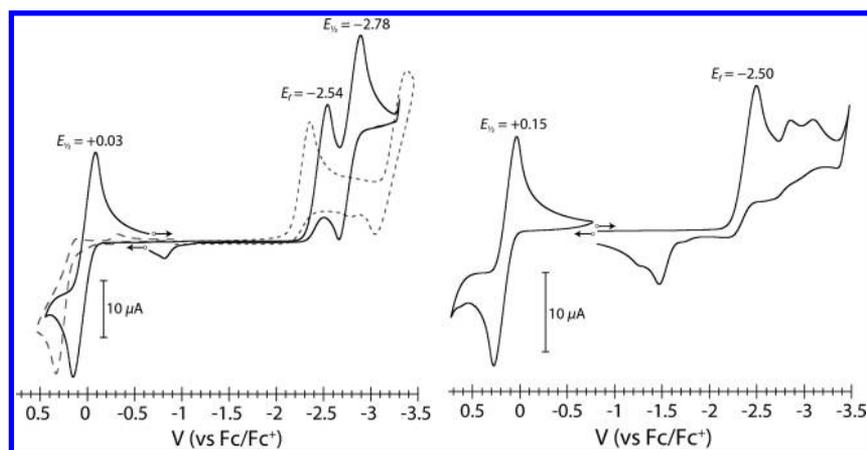

Figure 2. Cyclic voltammograms of **1^d-Cl** (left) and **2^d-Cl** (right) at a Pt electrode in THF. The scan rate is 50 mV/s, and the supporting electrolyte is 0.2 M Bu$_4$NPF$_6$. For compound **1^d-Cl**, the voltammogram of **1-Cl** under similar conditions is displayed for comparison (dashed gray line).

$[Co(N_2)(^{tBu}dPNP)]$ (**1^d-N$_2$**) (vide infra). As reported previously, chemical reduction of **1-Cl** generates the diamagnetic Co(I) species, $[Co(N_2)(^{tBu}PNP)]$ (**1-N$_2$**). We assign the irreversible cathode event at −2.54 V of **1^d-Cl** to an analogous reduction process that produces **1^d-N$_2$**. Upon further scanning to lower potentials, **1^d-N$_2$** is subsequently reduced in a reversible fashion to a new species. We assign this new species as a ligand-based radical anion on the basis of its reversible nature and its redox potential. As described above, the effect of dehydrogenation is to shift the potentials of all compounds of dPNP to more negative values compared with PNP. Therefore, a metal-based reduction to Co(0) would be expected to occur at a potential more negative than −3.13 V, where it is observed in the voltammogram for **1-Cl** (Figure 2). Additional cathode events are observed in cyclic voltammograms of **1^d-Cl** that may correspond to reduction to zerovalent cobalt, but they run up against the solvent window.

The EPR spectra of **1-Cl** and **1^d-Cl** were also investigated to determine whether dehydrogenation of the ligand backbone results in substantial changes to the nature of the unpaired spin in the Co(II) complexes. The spectra are displayed in Figure 3 and appear very similar for both compounds. At 30 K, both signals appear axial with resolved hyperfine coupling (ca. 400 MHz) to ^{59}Co in the $g_{\parallel}$ component. The g values of 3.67 and 1.82 for **1-Cl** and 3.62 and 1.82 for **1^d-Cl** are consistent with low-spin Co(II) species displaying spin orbit coupling in the ground state, as observed in other square-planar Co(II) complexes.[51,52] The similarity of the EPR spectra for both **1-Cl** and **1^d-Cl** is further consistent with their effective magnetic moments in solution of 2.1(2) and 1.8(2) μ_B, respectively. The
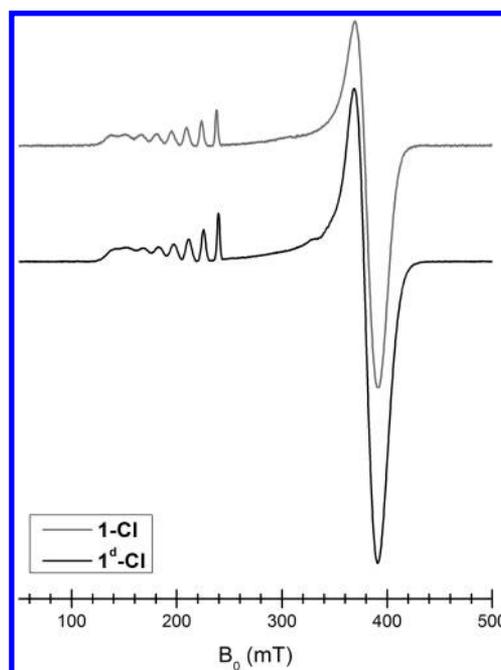

Figure 3. X-band EPR spectra of compounds **1-Cl** (upper) and **1^d-Cl** (lower) in a 2-MeTHF glass at 30 K.

unpaired spin in both compounds is localized on the cobalt center (vide infra) and therefore somewhat insensitive to minor changes in the chemical structure of the ligand backbone accounting for the nearly identical spectral envelope,

yet with an observable $g_{\parallel}$ value difference that translates to about a 2.5 mT shift in the magnetic field axis.

Reactivity. The change in redox potentials for 1^d-Cl versus 1-Cl next prompted us to explore the consequences of backbone modification on reactivity. In the case of nickel(II), the PNP platform has been demonstrated to stabilize a large range of organometallic compounds, including metal hydrides.[41,53] By contrast, analogous compounds with cobalt(II) have proven more difficult to prepare. The synthesis of the hydride complex, $[CoH(^{tBu}PNP)]$,[44] while known, is hampered by attendant reduction to give the cobalt(I) species, $[Co(N_2)(^{tBu}PNP)]$ (1-N$_2$).[36] Likewise, attempted synthesis of the cobalt(II) ethyl complex, $[Co(Et)(^{tBu}PNP)]$, in our hands resulted in similar reduction to 1-N$_2$. Recognizing the ~100 mV shift in reduction potential for 1^d-Cl versus 1-Cl, we therefore were curious to examine whether the dPNP ligand would prove more successful in permitting isolation of cobalt(II) complexes that are otherwise subject to reduction when supported by PNP.

Gratifyingly, treatment of 1^d-Cl with both KHBEt$_3$ and EtMgCl resulted in formation of the corresponding cobalt(II) hydride and ethyl species, respectively (1^d-H and 1^d-Et, eqs 2 and 3). In the former case, only trace evidence for formation of
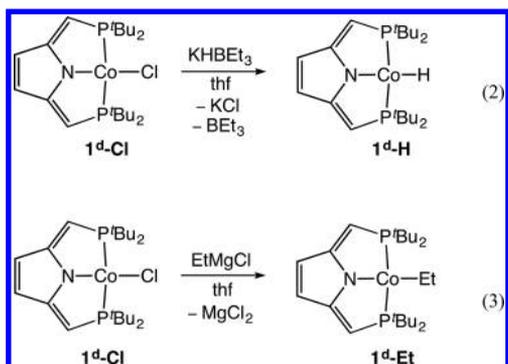
$[Co(N_2)(^{tBu}dPNP)]$ (1^d-N$_2$) was detected by NMR spectroscopy (<5%). Compound 1^d-N$_2$ could be prepared in rationale fashion by treatment of 1^d-Cl with one equivalent of KC$_8$ in THF (vide infra). The solid-state structure of compound 1^d-Et is shown in Figure 4. Much like 1^d-Cl, the structure of 1^d-Et is square-planar with very minimal deviation from planarity. The C−C distances about the backbone are similar to those of 1^d-Cl, while the Co−N distance displays a slight elongation, which is likely a consequence of the *trans* influence of the ethyl ligand. NMR spectra of 1^d-Et revealed the presence of small amounts of 1^d-H, indicating that β-H elimination is a likely decomposition pathway for the compound (see Supporting Information).

In similar fashion to 1-Cl, reduction of 1^d-Cl with KC$_8$ in THF generated the cobalt(I) dinitrogen complex, 1^d-N$_2$ (eq 4). Compound 1^d-N$_2$ is diamagnetic and displays ^{1}H and ^{13}C
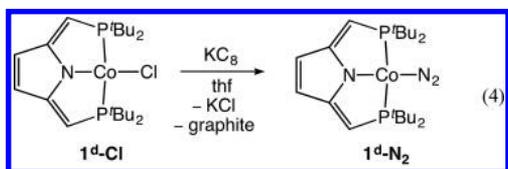
NMR features comparable to those of 2^d-Cl. The infrared stretch for the coordinated N$_2$ ligand was identified at 2012 cm^{-1}, which is similar but lower in energy to that found for 1-
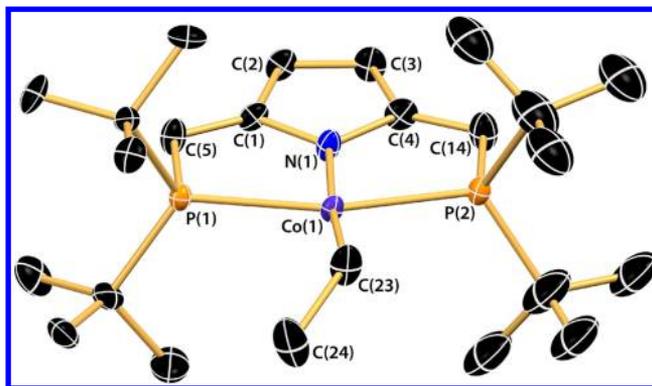
N$_2$ (2016 cm^{-1}), in line with the more reducing nature of dPNP vs PNP.[36] The solid-state structure of 1^d-N$_2$ is displayed in Figure 5. The bond metrics about Co are unremarkable, and the ligand shows the same bond alteration as that observed in 1^d-Cl.

Figure 4. Thermal ellipsoid (50%) drawing of 1^d-Et. Hydrogen atoms omitted for clarity. Selected bond distances (Å) and angles (deg): Co(1)−N(1) = 1.902(6); Co(1)−P(1) = 2.3107(16); Co(1)−P(2) = 2.2611(16); Co(1)−C(23) = 1.982(9); C(5)−C(1) = 1.350(10); C(1)−C(2) = 1.471(9); C(2)−C(3) = 1.349(10); P(1)−Co(1)−P(2) = 163.42(5); N(1)−Co(1)−C(23) = 173.6(4); Co(1)−C(23)−C(24) = 124.2(7).
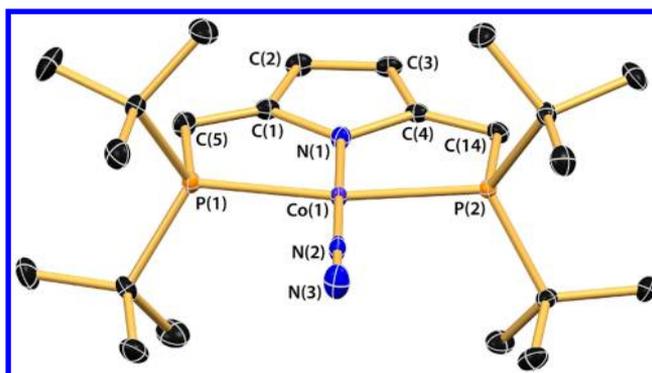
Figure 5. Thermal ellipsoid (50%) drawing of 1^d-N$_2$. Hydrogen atoms omitted for clarity. Selected bond distances (Å) and angles (deg): Co(1)−N(1) = 1.8645(15); Co(1)−P(1) = 2.2445(5); Co(1)−P(2) = 2.2487(5); Co(1)−N(2) = 1.7388(15); N(2)−N(3) = 1.126(2); C(5)−C(1) = 1.356(3); C(1)−C(2) = 1.473(2); C(2)−C(3) = 1.345(3); P(1)−Co(1)−P(2) = 164.78(2); N(1)−Co(1)−N(2) = 178.71(7); Co(1)−N(2)−N(3) = 179.10(17).

To verify the nature of the reversible cathode event observed in the voltammogram of 1^d-Cl (vide supra), we attempted the chemical reduction of 1^d-N$_2$. Treatment of 1^d-N$_2$ with one equivalent of KC$_8$ in THF gave rise to a new paramagnetic compound that we formulate as the cobalt dinitrogen complex containing a π-radical dianion PNP ligand (eq 5). This
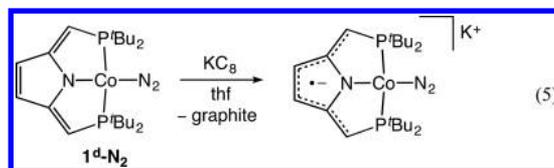
assignment is supported by a room temperature EPR signal observed at $g = 2.004$ for solutions of the complex generated in

situ (Figure 6). The isotropic spectrum displays rich hyperfine coupling to several different nuclei. Simulation of the signal

Figure 6. X-band EPR spectra and simulation of the radical observed from the reaction of 1^d-N_2 and KC_8 in THF. The first-derivative experimental spectrum and second harmonic are shown in black and blue, respectively. The theoretical reproduction of the experimental data is shown in red. The hyperfine and superhyperfine splitting pat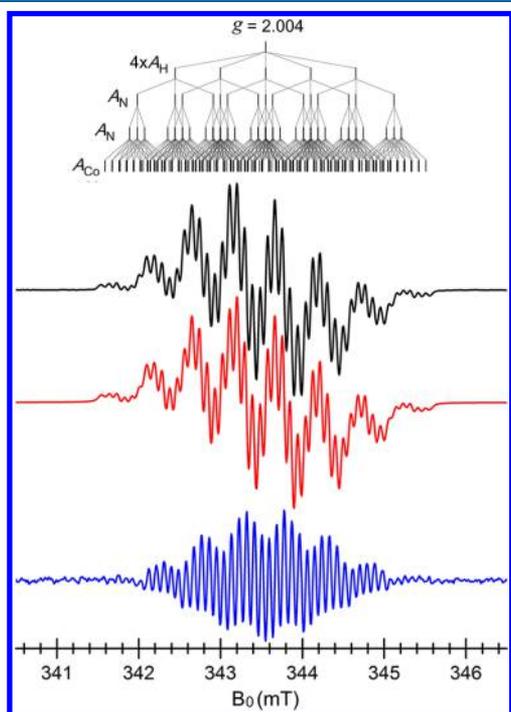tern used for the spectral simulation is shown at the top. The simulation parameters are as follows: a principal g value of 2.00413 split by four equivalent protons (A_H, 15.5 MHz), two inequivalent nitrogens (A_{N1}, 13.0 and A_{N2}, 2.6 MHz), and cobalt (A_{Co}, 2.4 MHz) with 0.085 mT line broadening. The spectra were collected at 298 K, 9.64 GHz microwave frequency, 1 mW microwave power, 100 kHz modulation frequency, 0.02 mT modulation amplitude, and an average of 9 scans.

was achieved with hyperfine interactions to four ^1H atoms (A = 15.5 MHz), two different ^{14}N atoms (A = 13.0 MHz and A = 2.6 MHz), and the ^{59}Co atom (A = 2.4 MHz), indicating a ligand-based radical with substantial delocalization about the π framework. The weaker of the two nitrogen hyperfine couplings is ascribed to the coordinating N atom of the dinitrogen ligand. Solution IR of the reduced product in THF displayed an NN stretch at 1974 cm^{-1}, further consistent with the assignment shown in eq 5 (see Supporting Information). A second minor NN stretch attributable to an unknown species was also observed for solutions of the reduced N_2 complex. Due to the sensitivity of the reduced product, its isolation was not pursued.

Based upon the reversible Co(II)/Co(III) couple observed by cyclic voltammetry, chemical oxidation of 1^d-Cl was also pursued to try and obtain a Co(III) complex of dPNP. Such a compound would be isoelectronic with the related Fe(II) complex, [FeCl(^{tBu}PNP)].[43] This compound is a rare example of square-planar iron(II) and possesses an intermediate spin (S = 1) ground state.[47] Reaction of 1^d-Cl with Ag(SbF$_6$) in methylene chloride led to an immediate color change from burgundy to light orange and formation of a new arene-

insoluble species that we assign as $[CoCl(^{tBu}dPNP)](SbF_6)$ (1^d-Cl$^+$, eq 6). ^1H NMR spectra of 1^d-Cl$^+$ in chloroform-d
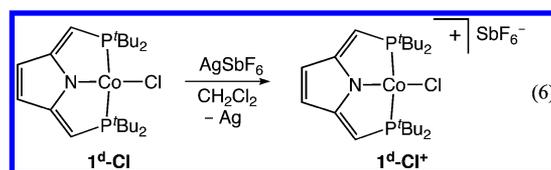
display three paramagnetically shifted resonances, consistent with C_{2v} symmetry in solution. Solution magnetic susceptibility measurements returned an effective magnetic moment of 3.6(2) μ_B in line with an S = 1 complex.[29,47,54] Although we have been unable to grow crystals of 1^d-Cl$^+$ suitable for complete structure refinement, low quality diffraction data permitted the connectivity of the molecular ion to be determined (see Supporting Information). Based on this data, the structure of 1^d-Cl$^+$ was found to be square-planar, analogous to the species reported by Schneider employing the dehydrogenated aliphatic PNP ligand.[29] Similar treatment of the Ni(II) analogue, 2^d-Cl, with AgSbF$_6$ failed to yield a tractable complex, perhaps due to further reactivity of the putative Ni(III) species.[55]

Computational Studies. To obtain more detailed insight into the electronic structure differences in 1-Cl and 1^d-Cl, spin-unrestricted DFT calculations were performed starting from the crystal structure coordinates, yielding good agreement between experiment and theory (Table 2) utilizing PBEPBE/

Table 2. Comparison of Experimental and Optimized Bond Lengths (Å) and Angles (deg) for 1^d-Cl and 1-Cl

	1^d-Cl		1-Cl	
bond metric	exptl	calc	exptl	calc
P(1)−Co	2.27204	2.274	2.25274	2.244
Co−P(2)	2.26673	2.273	2.24007	2.243
Co−N	1.84334	1.842	1.8626	1.859
Cl−Co	2.20573	2.206	2.20043	2.210
P(1)−Co-P(2)	165.472	166.7	167.529	168.0
Cl−Co−N	178.985	179.8	178.84	179.8
P(1)−Co−N	82.722	83.4	84.247	83.9
N−Co−P(2)	82.857	83.3	84.085	84.1

def2-TZVP. For both complexes, evaluation of molecular orbital (MO) character was subsequently conducted from the optimized geometries using spin-unrestricted B3LYP/def2-TZVP.

The calculated MO energy diagrams for 1^d-Cl and 1-Cl are given in Figure 7. Both the α and β orbitals are given for both compounds. Select frontier molecular orbital (FMO) depictions are also given in Figure 7 for the β FMOs of both complexes. For 1^d-Cl, the α FMOs exhibit dominant Co d character in the following orbitals: occupied α119, α122, α123, α124, and α125 as well as the unoccupied α129 orbital, where the observed d-character is assigned to d_{xy}, d_{xy}, d_{yz}, d_{xz}, d_{z^2}, $d_{x^2-y^2}$, respectively. In the β manifold, the FMOs exhibit dominant Co d character in the occupied β122, β123, β124, and β125 orbitals assigned as d_{xy}, d_{xz}, d_{xy}, and d_{z^2} respectively, as well as the unoccupied β128 and β129 orbitals assigned as d_{yz} and $d_{x^2-y^2}$, respectively. Note that there are two d_{xy} orbitals in both the α and β manifolds having high d-character and, hence, the highlighting of both in the MO analysis due to their similar d-orbital characters (note that the same challenge exists
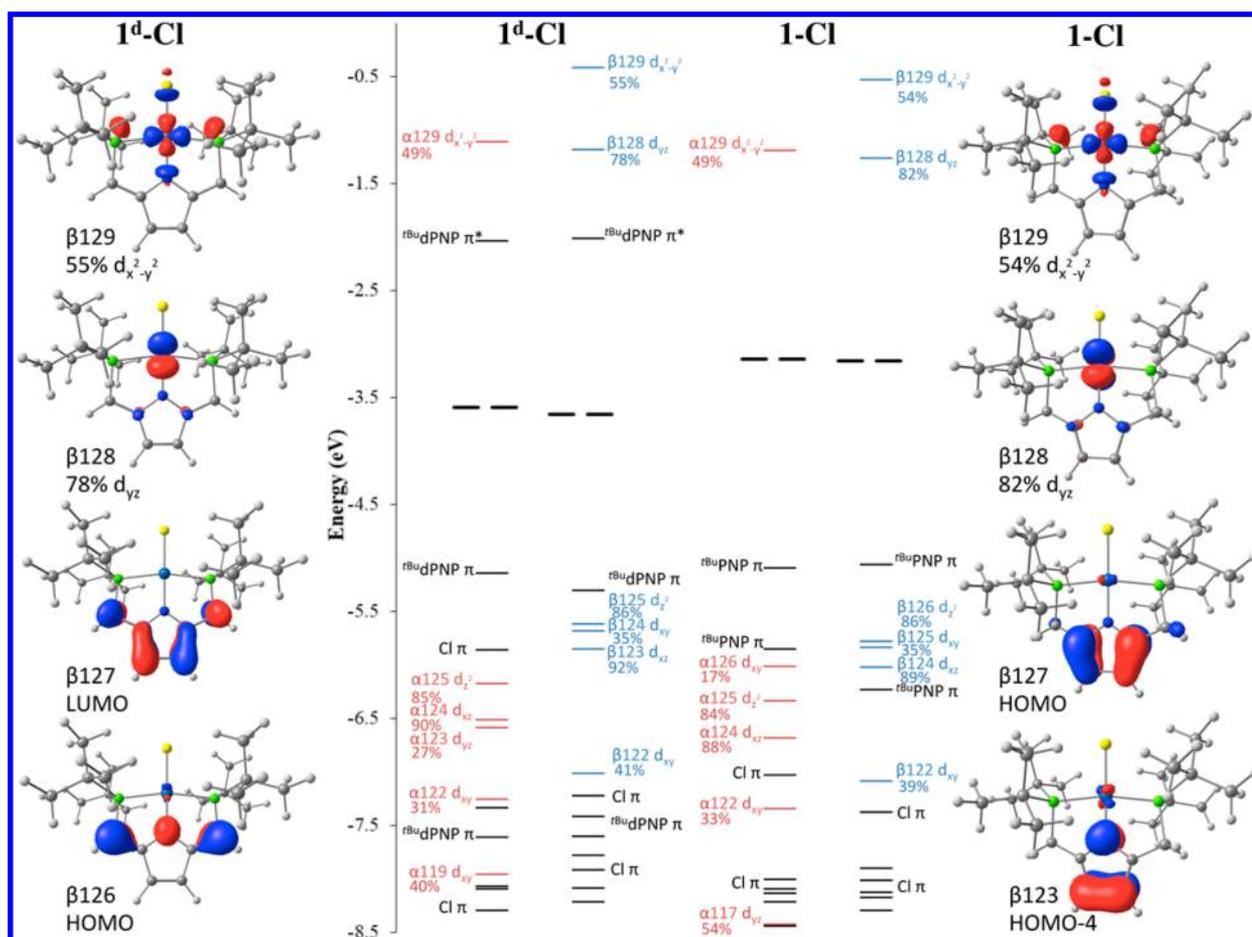
Figure 7. Calculated FMO diagrams for 1^d-Cl and 1-Cl. Selected β-orbital depictions are given for each complex.

for 1-Cl as well). Much like 1^d-Cl, in 1-Cl the α FMOs exhibiting dominant Co d character are occupied $\alpha117$, $\alpha122$, $\alpha124$, $\alpha125$, and $\alpha126$ as well as the unoccupied $\alpha129$ orbital, assigned as d_{yz}, d_{xy}, d_{xz}, d_{z^2}, d_{xy}, $d_{x^2-y^2}$, respectively. While in the β manifold, the FMOs exhibit dominant Co d character in the occupied $\beta122$, $\beta124$, $\beta125$, and $\beta126$ orbitals assigned as d_{xy}, d_{xz}, d_{xy}, and d_{z^2}, respectively, as well as the unoccupied $\beta128$ and $\beta129$ orbitals assigned as d_{yz} and $d_{x^2-y^2}$, respectively. Importantly, the LUMO of both the α and β manifolds in 1^d-Cl is a ^{tBu}dPNP π^* orbital, which is present as the HOMO of both the α and β manifolds in 1-Cl. Occupation of this orbital most likely accounts for the species observed upon reduction of 1^d-N$_2$ (vide supra), further underscored by the observed hyperfine pattern in Figure 6. Moreover, the UV−vis spectra for 1-Cl and 1^d-Cl display notable differences (see Supporting Information) consistent with distinct frontier MO structures for the compounds. With the exception of the difference in the LUMO, however, 1^d-Cl and 1-Cl exhibit similar MO diagrams in both the α and β manifolds, where $d_{x^2-y^2}$ is the highest energy unoccupied d orbital for both complexes displaying σ^* character to all atoms bound to the Co center as expected for a square-planar ligand field. Mayer bond order (MBO) and charge donation analyses (CDA) were also conducted for 1^d-Cl and 1-Cl and demonstrated only minor differences between the two complexes (see Supporting Information).

CONCLUSIONS

In this contribution, we demonstrated that treatment of Co and Ni complexes of ^{tBu}PNP with benzoquinone affords new

compounds with a dehydrogenated pincer ligand backbone. The net result of dehydrogenation is to create a more electron-rich ligand by disrupting the aromaticity of the pyrrole ring. The reactivity and electrochemistry of the resulting ^{tBu}dPNP complexes bears out this picture. In the case of Co(II), the implications of the backbone modification are marked, and complexes that have been challenging to prepare with the PNP ligand due to attendant reduction are isolated with only minimal reduction to Co(I) in the case of dPNP. Dehydrogenation of the pincer backbone also extends the π conjugation, resulting in new accessible ligand-based redox processes that were verified by chemical reduction of 1^d-N$_2$. Engaging such redox processes has been a target in pyrrole-based PNP ligands. Finally, DFT calculations were used to further probe the electronic structure of 1-Cl versus 1^d-Cl, confirming the presence of low-lying ligand-based frontier MOs in complexes of ^{tBu}dPNP. The use of the dPNP ligand in the design of new catalysts is the subject of ongoing investigation in our laboratory.

EXPERIMENTAL SECTION

General Comments. All manipulations were performed under an atmosphere of purified nitrogen gas using a Vacuum Atmospheres glovebox. Tetrahydrofuran, diethyl ether, pentane, and toluene were purified by sparging with argon and passage through two columns packed with 4 Å molecular sieves or activated alumina (THF and diethyl ether). Benzene-d_6 and chloroform-d were sparged with nitrogen gas and stored over 4 Å molecular sieves prior to use. ^{1}H NMR spectra were recorded on a Varian spectrometer operating at

300 or 500 MHz and referenced to the residual protium of the solvent. For selected paramagnetic compounds, only peak maxima are listed with full width at half-maximum (fwhm) values reported in hertz. ^{13}C NMR spectra were recorded at 125 MHz and referenced to the natural abundance ^{13}C atoms of the solvent. ^{31}P NMR spectra were recorded at 202 MHz and referenced automatically using the ^{2}H lock frequency. Electronic absorption spectra (UV−vis) were recorded on a Cary 60 spectrophotometer in toluene using airtight quartz cuvettes (path length = 10.0 mm) fitted with Teflon caps. FT-IR spectra were recorded with a ThermoNicolet iS 10 spectrophotometer as solid KBr pellets or in solution using an airtight liquid transmission cell (Specac OMNI) with KBr windows (path length = 0.05 mm). X-band EPR spectra were recorded on a Bruker E560 spectrometer in 4 mm o.d. quartz tubes at 9.64 GHz, 1 mW microwave power with 100 kHz modulation frequency. Low-spin Co(II) complexes were measured at 30 K with 0.6 mT modulation amplitude. Temperature control was maintained with a cryogen-free cryostat by an Oxford Mercury iTC. The Co(I) ligand anion radical was measured at room temperature with 0.02 mT modulation amplitude, average of nine scans. EPR simulation was performed with XEPR. Cyclic voltammetry was performed at 23 °C on a CH Instruments 620D electrochemical workstation. A 3-electrode setup was employed comprising a 1 mm Pt disk working electrode, platinum wire auxiliary electrode, and a Ag/AgCl quasi-reference electrode. Triply recrystallized Bu$_4$NPF$_6$ was used as the supporting electrolyte. All electrochemical data were referenced to the ferrocene/ferrocenium couple at 0.00 V. Solution magnetic susceptibility measurements were determined by the Evans method at 293 K without a solvent correction using reported diamagnetic corrections.[56,57] Elemental analyses were performed by the CENTC facility at the University of Rochester. In each case, recrystallized material was used for combustion analysis.

Crystallography. Crystals suitable for X-ray diffraction were mounted, using Paratone oil, onto a nylon loop. Data were collected at 98(2) K using a Rigaku AFC12/Saturn 724 CCD fitted with MoKα radiation ($\lambda = 71075$ Å). Low temperature data collection was accomplished with a nitrogen cold stream maintained by an X-Stream low-temperature apparatus. Data collection and unit cell refinement were performed using CrystalClear software.[58] Data processing and absorption correction, giving minimum and maximum transmission factors, were accomplished with CrysAlisPro[59] and SCALE3 ABSPACK,[60] respectively. The structure was solved with the ShelXT[61] structure solution program within Olex2[62] using direct methods and refined (on F^2) with the ShelXL package[63] using full-matrix, least-squares techniques. All non-hydrogen atoms were refined with anisotropic displacement parameters. All hydrogen atom positions were determined by geometry and refined by a riding model. The structure of $\mathbf{1^d}$-**Et** was solved in the space group $P1$, although the true space group is most likely $P\bar{1}$. Attempts to refine $\mathbf{1^d}$-**Et** in $P\bar{1}$ did not produce chemically reasonable structures.

Electronic Structure Calculations. Spin-unrestricted DFT calculations were performed with the Guassian 09 package.[64] All geometry optimization calculations were performed with the PBEPBE[65] exchange-correlation functional with the def2-TZVP[66,67] basis set generated from basis set exchange[68,69] on all atoms. The geometries of all complexes were fully optimized starting from X-ray crystal structures. All optimized geometries had frequencies found to be positive. Energies are given in the Supporting Information including zero-point and thermal corrections.

Further calculations of molecular orbitals used the B3LYP functional with the def2-TZVP basis set on all atoms. The analysis of MO compositions and Mayer bond orders was performed using AOMix program.[70,71] Orbitals from the Gaussian calculations were plotted with the ChemCraft program. Charge donation analysis was performed using AOMix-FO.[69]

Materials. Compounds **1-Cl** and **2-Cl** were prepared according to literature procedures.[40,44] KC$_8$ was synthesized by the method of Hegedus.[72] All other reagents were purchased from commercial suppliers and used as received.

[CoCl(^{tBu}dPNP)] ($\mathbf{1^d}$-Cl). To a stirred solution of 100 mg (0.21 mmol) of **1-Cl** in 7 mL of benzene was added 38 mg (0.36 mmol) of 1,4-benzoquinone as a solid in one portion. The reaction mixture was allowed to stir for 18 h at 23 °C. After this time, the mixture was filtered through Celite and evaporated to dryness. The burgundy product was then extracted into ∼10 mL of pentane and once again filtered through a plug of Celite. Crystallization from pentane at −30 °C afforded the product as 51 mg (51% yield) of brown crystals. NMR (C$_6$D$_6$): ^{1}H (300 MHz) δ 8.3 (36 tBu, 380 Hz), −25.6 (2 pyr−CH, 170 Hz), −44.9 (2 arm−CH, 550 Hz). μ_{eff} = 1.8(2) μ_B. Anal. Calcd for C$_{22}$H$_{40}$ClCoNP$_2$: C, 55.64; H, 8.49; N, 2.95. Found: C, 54.23; H, 8.40; N, 2.68.

[NiCl(^{tBu}dPNP)] ($\mathbf{2^d}$-Cl). To a stirred solution of 109 mg (0.23 mmol) of **2-Cl** in 7 mL of benzene was added 32 mg (0.30 mmol) of 1,4-benzoquinone as a solid in one portion. The reaction mixture was allowed to stir for 18 h at 23 °C. Afterward, the mixture was filtered through Celite and the resulting solution evaporated to dryness. The remaining residue was extracted into 10 mL of pentane. Subsequent filtration and crystallization at −30 °C afforded the product as 61 mg (56% yield) of red crystals. NMR (C$_6$D$_6$): ^{1}H (500 MHz) δ 6.36 (s, 2 pyr−CH), 4.13 (app t, J_{HP} = 2.2 Hz, 2 arm−CH), 1.52 (app t, J_{HP} = 6.8 Hz, 36 tBu); ^{13}C[^{1}H] δ 170.51 (app t, J_{CP} = 13.6 Hz), 131.60 (app t, J_{CP} = 6.8 Hz), 82.26 (app t, J_{CP} = 17.9 Hz), 36.65 (app t, J_{CP} = 7.9 Hz), 29.91; ^{31}P[^{1}H] δ 67.15. Anal. Calcd for C$_{22}$H$_{40}$ClNNiP$_2$: C, 55.67; H, 8.49; N, 2.95. Found: C, 55.96; H, 8.71; N, 2.82.

[CoH(^{tBu}dPNP)] ($\mathbf{1^d}$-H). A solution of 100 mg (0.21 mmol) of $\mathbf{1^d}$-**Cl** in 7 mL of THF was chilled to −30 °C. To the cooled solution was added 0.27 mmol of KHBEt$_3$ (1.0 M in THF) in a dropwise fashion. The reaction mixture was allowed to warm to 23 °C while stirring over the course of an hour. After this time, all volatiles were removed in vacuo, and the remaining residue was extracted into 10 mL of pentane. Subsequent filtration and evaporation to dryness furnished the product as 87 mg (94% yield) of a brown solid. The compound is quite soluble in pentane, and multiple attempts to crystallize the material resulted only in powders or noncrystalline residues. IR (KBr): cm^{-1} 1752 (ν_{CoH}). NMR (C$_6$D$_6$): ^{1}H (300 MHz) δ 12.6 (36 tBu, 450 Hz), −18.1 (2 pyr−CH, 63 Hz), −22.4 (2 arm−CH, 260 Hz). μ_{eff} = 2.1(2) μ_B. Repeated combustion analyses returned low values for carbon. Representative data is given. Anal. Calcd for C$_{22}$H$_{41}$CoNP$_2$: C, 59.99; H, 9.38; N, 3.18. Found: C, 53.94; H, 8.70; N, 2.56.

[CoEt(^{tBu}dPNP)] ($\mathbf{1^d}$-Et). To a stirred solution of 34 mg (0.072 mmol) of $\mathbf{1^d}$-**Cl** in 7 mL of THF was added 0.072 mmol of EtMgCl (1.0 M in THF) in one portion. The reaction mixture was allowed to stir at 23 °C for 3 h before being evaporated to dryness. The resulting residue was extracted into 5 mL of pentane and filtered through a plug of Celite. Chilling the pentane solution at −30 °C for 18 h afforded the target compound as 30 mg (89% yield) of brown crystals. NMR (C$_6$D$_6$): ^{1}H (300 MHz) δ 12.0 (36 tBu, 350 Hz), −18.8 (2 pyr−CH, 70 Hz), −29.1 (2 arm−CH, 220 Hz), −96.9 (3 CH_2CH_3, 550 Hz). μ_{eff} = 1.9(2) μ_B. Anal. Calcd for C$_{24}$H$_{45}$CoNP$_2$: C, 61.53; H, 9.68; N, 2.99. Found: C, 61.01; H, 9.47; N, 3.21.

[Co(N$_2$)(^{tBu}dPNP)] ($\mathbf{1^d}$-N$_2$). To a stirred solution of 100 mg (0.21 mmol) of $\mathbf{1^d}$-**Cl** in 7 mL of THF was added 28 mg (0.21 mmol) of KC$_8$ as a solid in one portion. The reaction mixture was allowed to stir at 23 °C for 16 h. After this time, the mixture was filtered through Celite, and all volatiles were removed in vacuo. The remaining residue was extracted into 10 mL of pentane. Subsequent filtration and evaporation to dryness furnished $\mathbf{1^d}$-N$_2$ as 98 mg (99%) of a brown solid. IR (THF): cm^{-1} 2012 (ν_{NN}). NMR (C$_6$D$_6$): ^{1}H (500 MHz) δ 6.42 (s, 2 pyr−CH), 4.34 (app t, J_{HP} = 2.2 Hz, 2 arm−CH), 1.47 (app t, J_{HP} = 6.0 Hz, 36 tBu); ^{13}C[^{1}H] δ 171.10 (app t, J_{CP} = 14.3 Hz), 131.33 (app t, J_{CP} = 6.4 Hz), 82.20 (app t, J_{CP} = 17.4 Hz), 36.63 (app t, J_{CP} = 7.6 Hz), 30.34; ^{31}P[^{1}H] δ 94.30. Anal. Calcd for C$_{22}$H$_{40}$CoN$_3$P$_2$: C, 56.53; H, 8.63; N, 8.99. Found: C, 56.75; H, 8.78; N, 9.01.

[CoCl(^{tBu}dPNP)](SbF$_6$) ($\mathbf{1^d}$-Cl$^+$). To a stirred solution of 155 mg (0.33 mmol) of $\mathbf{1^d}$-**Cl** in 7 mL of methylene chloride was added 123 mg (0.36 mmol) of AgSbF$_6$ as a solid in one portion. An immediate color change from burgundy to brown was observed, accompanied by

the formation of a precipitate. The reaction was allowed to stir for 1 h at 23 °C before being filtered through a plug of Celite. Concentration of the resulting solution to ~2 mL followed by addition of 10 mL of diethyl ether precipitated the product as 188 mg (81% yield) of a brown solid, which was subsequently washed with pentane. NMR (CDCl$_3$): ^{1}H (300 MHz) δ 51.1 (2 H, 27 Hz), 3.7 (2 H, 460 Hz), −13.8 (36 tBu, 28 Hz). μ_{eff} = 3.6(2) μ_B. Anal. Calcd for C$_{22}$H$_{40}$ClCoF$_6$NP$_2$Sb: C, 37.18; N, 5.67; N, 1.97. Found: C, 38.25; H, 5.62; N, 1.59. Slightly elevated values for carbon are the result of residual pentane from purification.

■ ASSOCIATED CONTENT

ⓢ Supporting Information

The Supporting Information is available free of charge on the ACS Publications website at DOI: 10.1021/acs.inorg-chem.8b01643.

> ^{1}H NMR, IR, and UV−vis spectra; ball and stick model of **1^d-Cl$^+$**; tables of crystallographic data and refinement parameters; tables of optimized atomic coordinates for **1-Cl** and **1^d-Cl** (PDF)

Accession Codes

CCDC 1846074−1846077 contain the supplementary crystallographic data for this paper. These data can be obtained free of charge via www.ccdc.cam.ac.uk/data_request/cif, by emailing data_request@ccdc.cam.ac.uk, or by contacting The Cambridge Crystallographic Data Centre, 12 Union Road, Cambridge CB2 1EZ, UK; fax: +44 1223 336033.

■ AUTHOR INFORMATION

Corresponding Author

*E-mail: zachary.tonzetich@utsa.edu.

ORCID ⓘ

Ian Davis: 0000-0002-1566-4972
Michael L. Neidig: 0000-0002-2300-3867
Aimin Liu: 0000-0002-4182-8176
Zachary J. Tonzetich: 0000-0001-7010-8007

Notes

The authors declare no competing financial interest.

■ ACKNOWLEDGMENTS

■ REFERENCES

(1) Szabó, K. Pincer Complexes as Catalysts in Organic Chemistry. *Top. Organomet. Chem.* **2013**, *40*, 203−241.

(2) Deng, Q. H.; Melen, R. L.; Gade, L. H. Anionic chiral tridentate N-donor pincer ligands in asymmetric catalysis. *Acc. Chem. Res.* **2014**, *47*, 3162−3173.

(3) Asay, M.; Morales-Morales, D. Non-symmetric pincer ligands: complexes and applications in catalysis. *Dalton Trans.* **2015**, *44*, 17432−17447.

(4) *Pincer Compounds: Chemistry and Applications*; Morales-Morales, D., Ed.; Elsevier: 2018.

(5) Gunanathan, C.; Milstein, D. Metal-Ligand Cooperation by Aromatization-Dearomatization: A New Paradigm in Bond Activation and ″Green″ Catalysis. *Acc. Chem. Res.* **2011**, *44*, 588−602.

(6) van der Vlugt, J. I. Cooperative Catalysis with First-Row Late Transition Metals. *Eur. J. Inorg. Chem.* **2012**, *2012*, 363−375.

(7) Lyaskovskyy, V.; de Bruin, B. Redox Non-Innocent Ligands: Versatile New Tools to Control Catalytic Reactions. *ACS Catal.* **2012**, *2*, 270−279.

(8) Zell, T.; Milstein, D. Hydrogenation and dehydrogenation iron pincer catalysts capable of metal-ligand cooperation by aromatization/dearomatization. *Acc. Chem. Res.* **2015**, *48*, 1979−1994.

(9) Chirik, P. J. Iron- and Cobalt-Catalyzed Alkene Hydrogenation: Catalysis with Both Redox-Active and Strong Field Ligands. *Acc. Chem. Res.* **2015**, *48*, 1687−1695.

(10) Chirik, P. J. Carbon−Carbon Bond Formation in a Weak Ligand Field: Leveraging Open-Shell First-Row Transition-Metal Catalysts. *Angew. Chem., Int. Ed.* **2017**, *56*, 5170−5181.

(11) Murugesan, S.; Kirchner, K. Non-precious metal complexes with an anionic PCP pincer architecture. *Dalton Trans.* **2016**, *45*, 416−439.

(12) *The Chemistry of Pincer Compounds*; Morales-Morales, D.; Jensen, C. G. M., Eds.; Elsevier B. V.: Amsterdam, 2007.

(13) Benito-Garagorri, D.; Kirchner, K. Modularly Designed Transition Metal PNP and PCP Pincer Complexes based on Aminophosphines: Synthesis and Catalytic Applications. *Acc. Chem. Res.* **2008**, *41*, 201−213.

(14) *Pincer and Pincer-Type Complexes*; Szabó, K.; Wendt, O. F., Eds.; Wiley-VCH Verlag Gmbh & Co.: Weinheim, Germany, 2014.

(15) Polezhaev, A. V.; Chen, C.-H.; Losovyj, Y.; Caulton, K. G. A Multifunctional Pincer Ligand Supports Unsaturated Cobalt: Five Functionalities in One Pincer. *Chem. - Eur. J.* **2017**, *23*, 8039−8050.

(16) Peris, E.; Crabtree, R. H. Key factors in pincer ligand design. *Chem. Soc. Rev.* **2018**, *47*, 1959−1968.

(17) Stegmann, H. B.; Scheffler, K.; Stöcker, F. Crystalline π-Radicals Containing Lead − Isotropic ^{207}Pb-ESR Hyperfine Structure. *Angew. Chem., Int. Ed. Engl.* **1970**, *9*, 456−456.

(18) Heyduk, A. F.; Zarkesh, R. A.; Nguyen, A. I. Designing Catalysts for Nitrene Transfer Using Early Transition Metals and Redox-Active Ligands. *Inorg. Chem.* **2011**, *50*, 9849−9863.

(19) Lu, F.; Zarkesh, R. A.; Heyduk, A. F. A Redox-Active Ligand as a Reservoir for Protons and Electrons: O2 Reduction at Zirconium-(IV). *Eur. J. Inorg. Chem.* **2012**, *2012*, 467−470.

(20) Hananouchi, S.; Krull, B. T.; Ziller, J. W.; Furche, F.; Heyduk, A. F. Metal effects on ligand non-innocence in Group 5 complexes of the redox-active [ONO] pincer ligand. *Dalton Trans.* **2014**, *43*, 17991−18000.

(21) Broere, D. L. J.; Plessius, R.; van der Vlugt, J. I. New avenues for ligand-mediated processes - expanding metal reactivity by the use of redox-active catechol, o-aminophenol and o-phenylenediamine ligands. *Chem. Soc. Rev.* **2015**, *44*, 6886−6915.

(22) Wang, X.; Yao, L.; Pan, Y.; Huang, K.-W. Synthesis of group 10 metal complexes with a new unsymmetrical PN3P-pincer ligand through ligand post-modification: Structure and reactivity. *J. Organomet. Chem.* **2017**, *845*, 25−29.

(23) Yao, C.; Wang, X.; Huang, K.-W. Nitrogen atom transfer mediated by a new PN^{3}P-pincer nickel core via a putative nitrido nickel intermediate. *Chem. Commun.* **2018**, *54*, 3940−3943.

(24) Wenz, J.; Vasilenko, V.; Kochan, A.; Wadepohl, H.; Gade, L. H. Coordination Chemistry of the PdmBOX Pincer Ligand: Reactivity at the Metal and the Ligand. *Eur. J. Inorg. Chem.* **2017**, *2017*, 5545−5556.

(25) Chang, M. C.; McNeece, A. J.; Hill, E. A.; Filatov, A. S.; Anderson, J. S. Ligand-Based Storage of Protons and Electrons in Dihydrazonopyrrole Complexes of Nickel. *Chem. - Eur. J.* **2018**, *24*, 8001−8008.

(26) McNeece, A. J.; Chang, M.-C.; Filatov, A. S.; Anderson, J. S. Redox Activity, Ligand Protonation, and Variable Coordination Modes of Diimino-Pyrrole Complexes of Palladium. *Inorg. Chem.* **2018**, *57*, 7044.

(27) Schneider, S.; Meiners, J.; Askevold, B. Cooperative Aliphatic PNP Amido Pincer Ligands − Versatile Building Blocks for

Coordination Chemistry and Catalysis. *Eur. J. Inorg. Chem.* **2012**, *2012*, 412−429.

(28) Schneck, F.; Finger, M.; Tromp, M.; Schneider, S. Chemical Non-Innocence of an Aliphatic PNP Pincer Ligand. *Chem. - Eur. J.* **2017**, *23*, 33−37.

(29) Lagaditis, P. O.; Schluschaß, B.; Demeshko, S.; Würtele, C.; Schneider, S. Square-Planar Cobalt(III) Pincer Complex. *Inorg. Chem.* **2016**, *55*, 4529−4536.

(30) Radosevich, A. T.; Melnick, J. G.; Stoian, S. A.; Bacciu, D.; Chen, C.-H.; Foxman, B. M.; Ozerov, O. V.; Nocera, D. G. Ligand Reactivity in Diarylamido/Bis(Phosphine) PNP Complexes of Mn(CO)₃ and Re(CO)₃. *Inorg. Chem.* **2009**, *48*, 9214−9221.

(31) Sekiguchi, Y.; Kuriyama, S.; Eizawa, A.; Arashiba, K.; Nakajima, K.; Nishibayashi, Y. Synthesis and reactivity of iron-dinitrogen complexes bearing anionic methyl- and phenyl-substituted pyrrole-based PNP-type pincer ligands toward catalytic nitrogen fixation. *Chem. Commun.* **2017**, *53*, 12040−12043.

(32) Nadif, S. S.; O'Reilly, M. E.; Ghiviriga, I.; Abboud, K. A.; Veige, A. S. Remote Multiproton Storage within a Pyrrolide-Pincer-Type Ligand. *Angew. Chem., Int. Ed.* **2015**, *54*, 15138−15142.

(33) Grüger, N.; Wadepohl, H.; Gade, L. H. A readily accessible PNP pincer ligand with a pyrrole backbone and its Ni^{I/II} chemistry. *Dalton Trans.* **2012**, *41*, 14028−14030.

(34) Kumar, S.; Mani, G.; Mondal, S.; Chattaraj, P. K. Pyrrole-Based New Diphosphines: Pd and Ni Complexes Bearing the PNP Pincer Ligand. *Inorg. Chem.* **2012**, *51*, 12527−12539.

(35) Venkanna, G. T.; Ramos, T. V. M.; Arman, H. D.; Tonzetich, Z. J. Nickel(II) Complexes Containing a Pyrrole-Diphosphine Pincer Ligand. *Inorg. Chem.* **2012**, *51*, 12789−12795.

(36) Krishnan, V. M.; Arman, H. D.; Tonzetich, Z. J. Preparation and reactivity of a square-planar PNP cobalt(II)-hydrido complex: isolation of the first {Co-NO}⁸-hydride. *Dalton Trans.* **2018**, *47*, 1435−1441.

(37) Thompson, C. V.; Davis, I.; DeGayner, J. A.; Arman, H. D.; Tonzetich, Z. J. Iron Pincer Complexes Incorporating Bipyridine: A Strategy for Stabilization of Reactive Species. *Organometallics* **2017**, *36*, 4928−4935.

(38) Thompson, C. V.; Arman, H. D.; Tonzetich, Z. J. A Pyrrole-Based Pincer Ligand Permits Access to Three Oxidation States of Iron in Organometallic Complexes. *Organometallics* **2017**, *36*, 1795−1802.

(39) Kessler, J. A.; Iluc, V. M. Ag(I) and Tl(I) Precursors as Transfer Agents of a Pyrrole-Based Pincer Ligand to Late Transition Metals. *Inorg. Chem.* **2014**, *53*, 12360−12371.

(40) Venkanna, G. T.; Arman, H. D.; Tonzetich, Z. J. Catalytic C−S Cross-Coupling Reactions Employing Ni Complexes of Pyrrole-Based Pincer Ligands. *ACS Catal.* **2014**, *4*, 2941−2950.

(41) Kreye, M.; Freytag, M.; Jones, P. G.; Williard, P. G.; Bernskoetter, W. H.; Walter, M. D. Homolytic H₂ cleavage by a mercury-bridged Ni(I) pincer complex [{(PNP)Ni}₂{μ-Hg}]. *Chem. Commun.* **2015**, *51*, 2946−2949.

(42) Levine, D. S.; Tilley, T. D.; Andersen, R. A. C−H Bond Activations by Monoanionic, PNP-Supported Scandium Dialkyl Complexes. *Organometallics* **2015**, *34*, 4647−4655.

(43) Kuriyama, S.; Arashiba, K.; Nakajima, K.; Matsuo, Y.; Tanaka, H.; Ishii, K.; Yoshizawa, K.; Nishibayashi, Y. Catalytic transformation of dinitrogen into ammonia and hydrazine by iron-dinitrogen complexes bearing pincer ligand. *Nat. Commun.* **2016**, *7*, 12181.

(44) Kuriyama, S.; Arashiba, K.; Tanaka, H.; Matsuo, Y.; Nakajima, K.; Yoshizawa, K.; Nishibayashi, Y. Direct Transformation of Molecular Dinitrogen into Ammonia Catalyzed by Cobalt Dinitrogen Complexes Bearing Anionic PNP Pincer Ligands. *Angew. Chem., Int. Ed.* **2016**, *55*, 14291−14295.

(45) Levine, D. S.; Tilley, T. D.; Andersen, R. A. Evidence for the Existence of Group 3 Terminal Methylidene Complexes. *Organometallics* **2017**, *36*, 80−88.

(46) Levine, D. S.; Tilley, T. D.; Andersen, R. A. Efficient and selective catalysis for hydrogenation and hydrosilation of alkenes and alkynes with PNP complexes of scandium and yttrium. *Chem. Commun.* **2017**, *53*, 11881−11884.

(47) Ehrlich, N.; Kreye, M.; Baabe, D.; Schweyen, P.; Freytag, M.; Jones, P. G.; Walter, M. D. Synthesis and Electronic Ground-State Properties of Pyrrolyl-Based Iron Pincer Complexes: Revisited. *Inorg. Chem.* **2017**, *56*, 8415−8422.

(48) Ehrlich, N.; Baabe, D.; Freytag, M.; Jones, P. G.; Walter, M. D. Pyrrolyl-based pincer complexes of iron − Synthesis and electronic structure. *Polyhedron* **2018**, *143*, 83.

(49) Nakajima, K.; Kato, T.; Nishibayashi, Y. Hydroboration of Alkynes Catalyzed by Pyrrolide-Based PNP Pincer−Iron Complexes. *Org. Lett.* **2017**, *19*, 4323−4326.

(50) Ghorai, D.; Mani, G. Unsubstituted quinoidal pyrrole and its reaction with oxygen, charge transfer and palladium(II) complexes via DDQ oxidation. *RSC Adv.* **2014**, *4*, 45603−45611.

(51) Semproni, S. P.; Milsmann, C.; Chirik, P. J. Four-Coordinate Cobalt Pincer Complexes: Electronic Structure Studies and Ligand Modification by Homolytic and Heterolytic Pathways. *J. Am. Chem. Soc.* **2014**, *136*, 9211−9224.

(52) Przyojski, J. A.; Arman, H. D.; Tonzetich, Z. J. NHC Complexes of Cobalt(II) Relevant to Catalytic C−C Coupling Reactions. *Organometallics* **2013**, *32*, 723−732.

(53) Venkanna, G. T.; Tammineni, S.; Arman, H. D.; Tonzetich, Z. J. Synthesis, Characterization, and Catalytic Activity of Ni(II) Alkyl Complexes Supported by Pyrrole- Diphosphine Ligands. *Organometallics* **2013**, *32*, 4656−4663.

(54) Hana, F.; Lough, A. J.; Lavoie, G. G. Coordinatively- and electronically-unsaturated square planar cobalt(III) complexes of a pyridine dianionic pincer ligand. *Dalton Trans.* **2017**, *46*, 16228−16235.

(55) Mondal, P.; Pirovano, P.; Das, A.; Farquhar, E. R.; McDonald, A. R. Hydrogen Atom Transfer by a High-Valent Nickel-Chloride Complex. *J. Am. Chem. Soc.* **2018**, *140*, 1834−1841.

(56) Sur, S. K. Measurement of magnetic susceptibility and magnetic moment of paramagnetic molecules in solution by high-field fourier transform NMR spectroscopy. *J. Magn. Reson.* **1989**, *82*, 169−173.

(57) Bain, G. A.; Berry, J. F. Diamagnetic Corrections and Pascal's Constants. *J. Chem. Educ.* **2008**, *85*, 532−536.

(58) *CrystalClear User's Manual*; Rigaku/MSC Inc., Rigaku Corporation: The Woodlands, TX, 2011.

(59) *CrysAlisPro*; Rigaku Oxford Diffraction, Rigaku Corporation: The Woodlands, TX, 2015; Vol. 1.171.38.41.

(60) *SCALE3 ABSPACK -An Oxford Diffraction Program*; Oxford Diffraction Ltd.: 2005; Vol. 1.0.4, gui:1.0.3.

(61) Sheldrick, G. SHELXT - Integrated space-group and crystal-structure determination. *Acta Crystallogr., Sect. A: Found. Adv.* **2015**, *71*, 3−8.

(62) Dolomanov, O. V.; Bourhis, L. J.; Gildea, R. J.; Howard, J. A. K.; Puschmann, H. OLEX2: a complete structure solution, refinement and analysis program. *J. Appl. Crystallogr.* **2009**, *42*, 339−341.

(63) Sheldrick, G. M. A short history of SHELX. *Acta Crystallogr., Sect. A: Found. Crystallogr.* **2008**, *64*, 112−122.

(64) Frisch, M. J.; Trucks, G. W.; Schlegel, H. B.; Scuseria, G. E.; Robb, M. A.; Cheeseman, J. R.; Scalmani, G.; Barone, V.; Mennucci, B.; Petersson, G. A.; Nakatsuji, H.; Caricato, M.; Li, X.; Hratchian, H. P.; Izmaylov, A. F.; Bloino, J.; Zheng, G.; Sonnenberg, J. L.; Hada, M.; Ehara, M.; Toyota, K.; Fukuda, R.; Hasegawa, J.; Ishida, M.; Nakajima, T.; Honda, Y.; Kitao, O.; Nakai, H.; Vreven, T.; Montgomery, Jr., J. A.; Peralta, J. E.; Ogliaro, F.; Bearpark, M. J.; Heyd, J.; Brothers, E. N.; Kudin, K. N.; Staroverov, V. N.; Kobayashi, R.; Normand, J.; Raghavachari, K.; Rendell, A. P.; Burant, J. C.; Iyengar, S. S.; Tomasi, J.; Cossi, M.; Rega, N.; Millam, N. J.; Klene, M.; Knox, J. E.; Cross, J. B.; Bakken, V.; Adamo, C.; Jaramillo, J.; Gomperts, R.; Stratmann, R. E.; Yazyev, O.; Austin, A. J.; Cammi, R.; Pomelli, C.; Ochterski, J. W.; Martin, R. L.; Morokuma, K.; Zakrzewski, V. G.; Voth, G. A.; Salvador, P.; Dannenberg, J. J.; Dapprich, S.; Daniels, A. D.; Farkas, Ö.; Foresman, J. B.; Ortiz, J. V.; Cioslowski, J.; Fox, D. J. *Gaussian 09*; Gaussian, Inc.: Wallingford, CT, 2009.

(65) Perdew, J. P.; Burke, K.; Ernzerhof, M. Generalized Gradient Approximation Made Simple. *Phys. Rev. Lett.* **1996**, *77*, 3865−3868.

(66) Weigend, F.; Ahlrichs, R. Balanced basis sets of split valence, triple zeta valence and quadruple zeta valence quality for H to Rn: Design and assessment of accuracy. *Phys. Chem. Chem. Phys.* **2005**, *7*, 3297−3305.

(67) Schäfer, A.; Huber, C.; Ahlrichs, R. Fully optimized contracted Gaussian basis sets of triple zeta valence quality for atoms Li to Kr. *J. Chem. Phys.* **1994**, *100*, 5829−5835.

(68) Feller, D. The role of databases in support of computational chemistry calculations. *J. Comput. Chem.* **1996**, *17*, 1571−1586.

(69) Schuchardt, K. L.; Didier, B. T.; Elsethagen, T.; Sun, L.; Gurumoorthi, V.; Chase, J.; Li, J.; Windus, T. L. Basis Set Exchange: A Community Database for Computational Sciences. *J. Chem. Inf. Model.* **2007**, *47*, 1045−1052.

(70) Gorelsky, S. I.: *AOMix−Software Package for Electronic Structure Analysis*, Revision 6.85; http://www.sg-chem.net, Ottawa, ON, 2014.

(71) Gorelsky, S. I.; Lever, A. B. P. Electronic structure and spectra of ruthenium diimine complexes by density functional theory and INDO/S. Comparison of the two methods. *J. Organomet. Chem.* **2001**, *635*, 187−196.

(72) Schwindt, M. A.; Lejon, T.; Hegedus, L. S. Improved synthesis of (aminocarbene)chromium(0) complexes with use of C_8K-generated $Cr(CO)_5^{2-}$. Multivariant optimization of an organometallic reaction. *Organometallics* **1990**, *9*, 2814−2819.